arXiv:1409.3201v1 [cond-mat.mes-hall] 10 Sep 2014

From dissipative dynamics to studies of heat transfer at the nanoscale

Nazim Boudjada[1,2] and Dvira Segal[2]
[1] *Ecole Polytechnique de Montreal, Montreal, Quebec, Canada H3C 3A7 and*
[2] *Chemical Physics Theory Group, Department of Chemistry, University of Toronto, 80 Saint George St. Toronto, Ontario, Canada M5S 3H6*

(Dated: September 11, 2014)

We study in a unified manner the dissipative dynamics and the transfer of heat in the two-bath spin-boson model. We use the Bloch-Redfield (BR) formalism, valid in the very weak system-bath coupling limit, the noninteracting-blip approximation (NIBA), applicable in the non-adiabatic limit, and iterative, numerically-exact path integral tools. These methodologies were originally developed for the description of the dissipative dynamics of a quantum system, and here they are applied to explore the problem of quantum energy transport in a non-equilibrium setting. Specifically, we study the weak-to-intermediate system-bath coupling regime at high temperatures $k_BT/\hbar > \epsilon$, with ϵ as the characteristic frequency of the two-state system. The BR formalism and NIBA can lead to close results for the dynamics of the reduced density matrix (RDM) in a certain range of parameters. However, relatively small deviations in the RDM dynamics propagate into significant qualitative discrepancies in the transport behavior. Similarly, beyond the strict non-adiabatic limit NIBA's prediction for the heat current is qualitatively incorrect: It fails to capture the turnover behavior of the current with tunneling energy and temperature. Thus, techniques that proved meaningful for describing the RDM dynamics, to some extent even beyond their rigorous range of validity, should be used with great caution in heat transfer calculations, since qualitative-serious failures develop once parameters are mildly stretched beyond the techniques' working assumptions.

PACS numbers:

I. INTRODUCTION

Quantum impurity models, comprising a subsystem in an environment, embody complex processes in condensed phases: electron and exciton transfer in solids, solutions, glasses and biomolecules [1, 2], screening of a magnetic impurity by the Fermi sea electrons [3], electronic conduction of molecules [2], and the decoherence behavior of superconducting qubits [3, 4]. The dissipative dynamics of impurity models has been explored intensively by time-evolving the subsystem (reduced) density matrix, revealing mechanisms of decoherence and relaxation towards equilibrium. Here, as a case study, we focus on the spin-boson (SB) model with a two-level system (TLS) immersed in a bath of harmonic oscillators [1].

Beyond the question of decoherence and dissipation, impurity models can be employed for exploring fundamentals of quantum transport and quantum thermodynamics, when placing the subsystem between two reservoirs maintained e.g. at different chemical potentials or temperatures. In this scenario, the reservoirs exchange charge, spin, or energy carriers through the subsystem, with quantities of interest as (charge, energy, spin) currents in the system, as well as high order cumulants of currents. In the context of nanoscale heat transfer and phononics [5–7], the "non-equilibrium spin-boson model" (NESB), with a TLS bridging two thermal reservoirs at different temperatures, has been suggested as a toy model for studying the phenomenology of quantum heat transfer in anharmonic junctions [8], see Fig. 1 for a schematic representation.

The dissipative dynamics of the SB model has been examined systematically by comparing predictions from different techniques. Results have been organized in several reviews [1, 3], and the problem still provides an active area for exploration, see for example Refs. [9–12]. In contrast, the analysis of heat transfer characteristics in the corresponding NESB model is a relatively new problem and a systematic comparison of results from different techniques is still missing. One should note that the computation of transport characteristics in the NESB model (and other non-equilibrium impurity models) relies on a nontrivial extension of open quantum systems methodologies: To calculate the current one needs to follow the dynamics of other operators beyond the reduced density matrix (RDM): two-time correlation functions of subsystem's operators or expectation values of bath operators. The thermal properties of the NESB nanojunction have been analyzed on the basis of perturbative quantum master equations [8, 13–17], Keldysh Green's function expansions, [18–21], and the noninteracting-blip approximation [8, 22, 23]. Numerically exact techniques, developed for the study of the (single-bath) SB model, were similarly generalized to explore transport properties: the multilayer multiconfiguration time-dependent Hartree theory [24], influence functional path integral techniques [25] and Monte-Carlo simulations [26].

Theoretical studies of heat flow in model systems such as the NESB nanojunction are motivated by recent experiments of thermal energy flow across alkane chains [27–29], proteins [30] and small aromatic molecules [31–34].

These studies aim in exploring the role of vibrational energy flow in e.g. chemical reaction dynamics, protein folding, conformational changes, and molecular electronics. Questions of phononic heat transfer are of great interest in other disciplines. For example, in thermoelectric applications reducing the phononic contribution to the thermal conductivity improves the (heat to work) conversion efficiency; recent experiments reached reduced thermal conductivities in nanocomposites [35]. It is particularly interesting to design a molecular-level or a nanoscale thermal diode, optimally commanding unidirectional energy flow. This would allow control over molecular reactivity, and potentially turn into a building block in phononic (and similarly photonic) devices. Unidirectional heat flow was recently demonstrated in nitrobenzene [32]: Using ultrafast infrared Raman spectroscopy it was shown that energy transfer from the nitro to the phenyl group, or from the nitro to global vibrational modes, was blocked. However, vibrational energy was transferred from the phenyl-localized modes to the nitro modes and to global modes. It is now established that control over quantum energy flow can be achieved by combining many-body interactions with spatial asymmetries [7, 8]. Anharmonicity of vibrational modes is thus an essential ingredient for building nontrivial functionalities. While more detailed calculations are imperative to explore particular systems [36, 37], the NESB model with a two-level system, a truncated harmonic vibration, is the simplest-nontrivial model which can allow us to explore the role of anharmonic (many-body) effects in phononic (or photonic) conduction.

In this work, we are interested in the problem of quantum heat transfer in anharmonic nanojunctions, particularly when the central object's coupling energy to the contacts is substantial. Our goal is to examine and compare different techniques, understand their range of validity, and find out when they provide qualitatively correct results in comparison to exact numerical techniques. Focusing on the NESB model, we aim in rectifying the following points:

(i) Relation between dissipative dynamics and transport. We study here both the RDM dynamics and the transfer of heat in the NESB model using the weak-coupling (system-bath) Bloch-Redfield (BR) formalism, the noninteracting-blip approximation (NIBA), valid in the non-adiabatic limit and at high temperatures, and numerically-exact influence-functional path integral simulations. The BR and NIBA techniques provide consistent results when describing the dynamics of the RDM in a certain range of parameters. Does this agreement translate into consistent transport properties? The answer is negative. We show here that even when the BR and NIBA techniques reasonably agree on the RDM dynamics, results significantly deviate when following the heat current behavior: The BR scheme fails in providing the current characteristics, qualitatively and quantitatively, beyond the very weak coupling limit. Similarly, beyond the strict non-adiabatic limit NIBA badly fails in describing transport trends, while it still performs reasonably well in RDM calculations.

(ii) Developing approaches for weak-intermediate coupling cases. The BR method administers quantum kinetic equations, and it provides a transparent theory for thermal conduction: a linear enhancement of current with increasing coupling energy to the contacts. Other methods reveal that this trend breaks down immediately beyond the very weak coupling limit [18, 21, 22, 25, 26]. However, a careful comparison between different techniques is missing. To study physical situations, e.g., with the molecule moderately or strongly attached to thermal contacts as in Ref. [29], it is imperative to develop reliable methodologies that can extend beyond the very weak coupling regime. We play here with four different approaches, BR [8, 14, 38], NIBA [8, 22], perturbative techniques based on non-equilibrium Green's function (NEGF) [18, 21], and numerically exact influence functional path-integral simulations [25]. We study the current characteristics as a function of the contact interaction, as well as the temperature and the frequency of the TLS, and observe a nontrivial non-monotonic performance of the junction, exposing the underlying mechanisms of thermal conduction.

The paper is organized as follows. In Sec. II we present the model and observables of interest: the reduced density matrix and the heat current, including the linear response coefficient, the thermal conductance. In Sec. III we lay down the Bloch-Redfield equations for the RDM and the steady-state current. Sec. IV presents the corresponding NIBA equations. Sec. V describes influence functional path integral approaches. Numerical results for the RDM dynamics and steady-state heat current are included in Sec. VI. In Sec. VII we summarize our work.

II. MODEL AND OBSERVABLES OF INTEREST

The NESB model includes a two-state system (spin) bridging two bosonic reservoirs ($\nu = L, R$). In the "local" basis ($|0\rangle$ and $|1\rangle$) the isolated spin Hamiltonian reads

$$H_0 = \frac{\hbar\omega_0}{2}\sigma_z + \frac{\hbar\Delta}{2}\sigma_x, \tag{1}$$

and the total Hamiltonian is given by

$$H = H_0 + \sum_{\nu,k}\left[\frac{\hbar\sigma_z}{2}\lambda_{k,\nu}(b^\dagger_{k,\nu} + b_{k,\nu}) + \hbar\omega_k b^\dagger_{k,\nu}b_{k,\nu}\right]. \tag{2}$$

The Pauli matrices are defined as $\sigma_z = |1\rangle\langle 1| - |0\rangle\langle 0|$, $\sigma_x = |0\rangle\langle 1| + |1\rangle\langle 0|$, and $\sigma_y = -i|1\rangle\langle 0| + i|0\rangle\langle 1|$, $\hbar\omega_0$ is the level detuning (bias), Δ stands for the tunneling frequency between the spin states, and $b^\dagger_{k,\nu}$ ($b_{k,\nu}$) is the creation (annihilation) operator of a boson (e.g. phonon) with a wavenumber k in the ν reservoir. The interaction of the subsystem with the baths can be characterized by a spectral density function, defined as

$$J_\nu(\omega) = \sum_k \lambda^2_{k,\nu}\, \delta(\omega - \omega_k). \tag{3}$$

We perform our numerical simulations using an Ohmic form,

$$J_\nu(\omega) = 2\alpha_\nu \omega e^{-\omega/\omega_c}. \tag{4}$$

The methodologies discussed below can handle other spectral functions. Here α_ν is a dimensionless interaction parameter between the spin subsystem and the ν reservoir. Below we use the definition $\alpha \equiv \alpha_L + \alpha_R$. For simplicity, the cutoff frequency ω_c is taken identical in both baths. In the context of electron transfer processes it is useful to define the reorganization energy $E^\nu_r \equiv \int d\omega J_\nu(\omega)/\omega$. For Ohmic functions it reduces to $E^\nu_r = 2\alpha_\nu\omega_c$.

Below we principally work in the so-called non-adiabatic limit of $\Delta/\omega_c \ll 1$ and temperatures $k_BT/\hbar\Delta \gtrsim 1$. The "non-adiabatic" terminology is delivered from studies of electron transfer reactions in condensed phases, in which the TLS represents electron-donor and acceptor states with a tunneling frequency Δ: "adiabatic processes" $\Delta > \omega_c$ refer to reactions with fast tunneling electrons relative to the phonon bath. In the opposite non-adiabatic limit $\Delta \ll \omega_c$ the characteristic time scale of the bath $1/\omega_c$ is short relative to the internal timescale for tunneling.

Based on transport results in this range, we identify four regions: (i) we refer below to $\alpha_\nu < 0.025$ as the very weak coupling regime, (ii) $0.025 < \alpha_\nu < 0.1$ corresponds to the weak coupling limit, (iii) $0.1 < \alpha_\nu < 0.5$ describes the intermediate regime, and (iv) $\alpha_\nu > 0.5$ corresponds to the strong coupling limit.

The reduced density matrix is organized from the population difference $\langle\sigma_z(t)\rangle$ and the real and imaginary parts of the coherence $\langle\sigma_{x,y}(t)\rangle$,

$$\langle\sigma_i(t)\rangle = \mathrm{tr}\{\rho(t=0)e^{iHt/\hbar}\sigma_i e^{-iHt/\hbar}\}, \tag{5}$$

with $\rho(t=0)$ as the initial state of the total density matrix. In what follows we assume a factorized initial condition, $\rho(t=0) = \rho_L \otimes \rho_R \otimes |1\rangle\langle 1|$. The two reservoirs, $H_\nu = \sum_k \hbar\omega_k b^\dagger_{k,\nu} b_{k,\nu}$, are separately prepared in a canonical-equilibrium state of temperature $T_\nu = 1/(k_B\beta_\nu)$,

$$\rho_\nu = \frac{e^{-\beta_\nu H_\nu}}{Z_\nu}, \quad Z_\nu = \mathrm{Tr}_\nu e^{-\beta_\nu H_\nu}. \tag{6}$$

At $t = 0$ the subsystem-bath interaction is turned on and we wait for the (assuming unique) steady-state solution to set in. The heat current can be computed from the transient regime to the steady-state limit; below we focus only on the long-time behavior. It is reached by considering energy leakage at the contacts. For example, at the left contact the heat current operator is defined as

$$\hat{j}_L \equiv \frac{dH_L}{dt} = \frac{i}{\hbar}[H, H_L]. \tag{7}$$

Tracing over all degrees of freedom we reach the expectation value

$$j_L \equiv \mathrm{tr}[\rho(t=0)\hat{j}_L(t)]. \tag{8}$$

Operators are written here in the Heisenberg representation. In steady-state, $j_q = j_L = -j_R$. In the linear response regime the current is expanded to the lowest order in the temperature difference, $j_q \sim \kappa(T_L - T_R)$, and we obtain the thermal conductance κ from the relation

$$\kappa \equiv \frac{dj_q}{dT_L}\Big|_{T_L \to T_R = T}. \tag{9}$$

To practically compute the heat current we wish to manipulate Eq. (8) into a workable definition. A formally-exact construction has been derived in Ref. [18] from the perturbation expansion of the non-equilibrium Green's function. This formula, a many-body extension of Landauer's expression [39], an analog of the Meir-Wingreen formula for electronic systems [40], expresses the heat current of the NESB model in correlation functions of the spin. The linear response limit of this formula was recently studied using Monte-Carlo simulations to explore signatures of Kondo physics in thermal conduction [26]. In the following sections we describe the evaluation of the heat current within different sets of approximations.

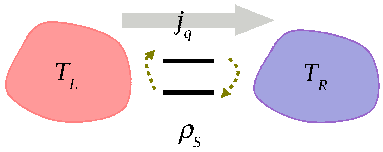

FIG. 1: Scheme of the non-equilibrium spin-boson model, a minimal picture for studying heat transport in anharmonic nano-junctions. In this work we simulate both the dynamics of the (spin) reduced density matrix ρ_S and the heat current behavior j_q using approximate methods and numerically exact simulation tools.

III. BLOCH-REDFIELD FORMALISM: VERY WEAK COUPLING REGIME

A. Hamiltonian

The standard Bloch-Redfield equation can be derived from the exact quantum master equation based on the assumption of weak system-bath interactions. It is convenient to develop it in the "energy" basis, the representation in which the spin subsystem is diagonal,

$$H_S = \sum_n E_n |n\rangle\langle n|. \tag{10}$$

In addition, the total Hamiltonian should be prepared in an additive structure,

$$\tilde{H} = H_S + H_L + H_R + V_L + V_R, \tag{11}$$

with the thermal baths denoted each by H_ν and the system-bath interaction given in a direct-product form,

$$\begin{aligned} V_\nu &= S^\nu \otimes B_\nu, \\ S^\nu &= \sum_{n,n'} S^\nu_{n,n'} |n\rangle\langle n'|. \end{aligned} \tag{12}$$

Here B_ν and S^ν are bath and subsystem operators, respectively. We label the subsystem operator by the index $\nu = L, R$; the impurity may couple to the two baths via distinct operators.

Specifically to the NESB model, we diagonalize the isolated TLS of Eq. (1) with a rotation matrix $U = e^{-\frac{i}{2}\theta\sigma_y}$, $\tan\theta = \Delta/\omega_0$. The total Hamiltonian (2) transforms into $\tilde{H} \equiv U^\dagger H U$, with

$$\begin{aligned} \tilde{H} &= \frac{\hbar\epsilon}{2}\tilde{\sigma}_z + \sum_{\nu,k} \hbar\omega_k b^\dagger_{k,\nu} b_{k,\nu} \\ &+ \frac{1}{2}\left(\hbar\tilde{\sigma}_z\cos\theta - \hbar\tilde{\sigma}_x\sin\theta\right)\sum_{\nu,k}\lambda_{k,\nu}(b^\dagger_{k,\nu} + b_{k,\nu}), \end{aligned} \tag{13}$$

where $\epsilon = \sqrt{\omega_0^2 + \Delta^2}$ and $\tilde{\sigma}_i$ are the Pauli matrices in the energy basis, denoted here by $|\pm\rangle$. We now identify the operators of Eq. (12) by

$$\begin{aligned} S^\nu &= \tilde{\sigma}_z\cos\theta - \tilde{\sigma}_x\sin\theta, \\ B_\nu &= \frac{1}{2}\sum_k \hbar\lambda_{k,\nu}(b^\dagger_{k,\nu} + b_{k,\nu}). \end{aligned} \tag{14}$$

The dynamics of the reduced density matrix under the BR equation has been examined in numerous studies [3, 43]. For completeness, we include in Sec. III B relevant expressions using a notation similar to that employed in Ref. [9]. The heat current in the NESB model was only recently derived in a closed form at the level of the BR scheme [14, 38]. A workable expression is provided in Sec. III C.

B. Reduced density matrix

In the BR scheme the interaction V_ν is treated perturbatively, to the lowest nontrivial order [41]. This results in a master equation for the spin RDM [42]. It obeys an integro-differential equation, written here in the local-site basis

of Eq. (2) [9, 42, 43],

$$\begin{aligned}
\frac{d}{dt}\langle\sigma_z(t)\rangle &= \Delta\langle\sigma_y(t)\rangle, \\
\frac{d}{dt}\langle\sigma_y(t)\rangle &= \omega_0\langle\sigma_x(t)\rangle - \Delta\langle\sigma_z(t)\rangle - \int_0^t d\tau G_y(\tau) - \int_0^t d\tau \left[G_{yy}(\tau)\langle\sigma_y(t-\tau)\rangle + G_{yx}(\tau)\langle\sigma_x(t-\tau)\rangle\right], \\
\frac{d}{dt}\langle\sigma_x(t)\rangle &= -\omega_0\langle\sigma_y(t)\rangle - \int_0^t d\tau G_x(\tau) - \int_0^t d\tau \left[G_{xx}(\tau)\langle\sigma_x(t-\tau)\rangle - G_{yx}(\tau)\langle\sigma_y(t-\tau)\rangle\right].
\end{aligned} \tag{15}$$

The kernels satisfy

$$\begin{aligned}
G_x(t) &= \frac{\Delta}{\epsilon}\sin(\epsilon t)\sum_\nu M''_\nu(t), \quad G_y(t) = \frac{\omega_0\Delta}{\epsilon^2}\left[1-\cos(\epsilon t)\right]\sum_\nu M''_\nu(t) \\
G_{xx}(t) &= \cos(\epsilon t)\sum_\nu M'_\nu(t), \quad G_{yy}(t) = \frac{\Delta^2+\omega_0^2\cos(\epsilon t)}{\epsilon^2}\sum_\nu M'_\nu(t) \\
G_{yx}(t) &= \frac{\omega_0}{\epsilon}\sin(\epsilon t)\sum_\nu M'_\nu(t),
\end{aligned} \tag{16}$$

and the dissipative terms enclose the correlation function $\langle B_\nu(t)B_\nu(0)\rangle_\nu = M'_\nu(t) - iM''_\nu(t)$, with

$$\begin{aligned}
M'_\nu(t) &= \int_0^\infty d\omega J_\nu(\omega)\coth(\beta_\nu\hbar\omega/2)\cos(\omega t), \\
M''_\nu(t) &= \int_0^\infty d\omega J_\nu(\omega)\sin(\omega t).
\end{aligned} \tag{17}$$

Under the Markov approximation, we write a time-local Markovian equation $d\langle\sigma_i\rangle/dt = \sum_{i,j} D_{i,j}\sigma_j$, see e.g. [9, 42, 44], and solve it in the long time limit. The equilibrium (eq) solution, in the case of a single bath, is $\langle\sigma_z\rangle_{eq} = -\frac{\omega_0}{\epsilon}\tanh(\beta\hbar\epsilon/2)$, $\langle\sigma_x\rangle_{eq} = -\frac{\Delta}{\epsilon}\tanh(\beta\hbar\epsilon/2)$, and $\langle\sigma_y\rangle_{eq} = 0$. In the non-equilibrium two-bath scenario the steady-state (ss) solution of the Markovian equation (reached at $t\to\infty$) satisfies

$$\begin{aligned}
\langle\sigma_z\rangle_{ss} &= -\frac{\omega_0}{\epsilon}\frac{J_L(\epsilon)+J_R(\epsilon)}{J_L(\epsilon)\coth(\beta_L\hbar\epsilon/2)+J_R(\epsilon)\coth(\beta_R\hbar\epsilon/2)}, \\
\langle\sigma_x\rangle_{ss} &= \frac{\Delta}{\omega_0}\langle\sigma_z\rangle_{ss}, \\
\langle\sigma_y\rangle_{ss} &= 0,
\end{aligned} \tag{18}$$

reducing to the correct equilibrium state [3]. These elements build-up the reduced density matrix,

$$\rho_S^{ss} = \frac{1}{2}\begin{pmatrix} 1+\langle\sigma_z\rangle_{ss} & \langle\sigma_x\rangle_{ss} - i\langle\sigma_y\rangle_{ss} \\ \langle\sigma_x\rangle_{ss} + i\langle\sigma_y\rangle_{ss} & 1-\langle\sigma_z\rangle_{ss}\end{pmatrix}. \tag{19}$$

We now introduce a short notation, $x \equiv \frac{J_L(\epsilon)+J_R(\epsilon)}{J_L(\epsilon)\coth(\beta_L\hbar\epsilon/2)+J_R(\epsilon)\coth(\beta_R\hbar\epsilon/2)}$, and condense the RDM into

$$\rho_S^{ss} = \frac{1}{2}\hat{I} - \frac{x}{\epsilon}\left(\frac{\omega_0}{2}\sigma_z + \frac{\Delta}{2}\sigma_x\right). \tag{20}$$

Here $\hat{I}$ stands for the identity matrix. In the energy basis $|\pm\rangle$, $\tilde{\rho}_S^{ss} = U^\dagger\rho_S^{ss}U$, resulting in the simple form

$$\tilde{\rho}_S^{ss} = \frac{1}{2}\hat{I} - \frac{x}{2}\tilde{\sigma}_z. \tag{21}$$

Explicitly, the population of the two levels in the energy basis follows

$$\begin{aligned}
\tilde{p}_-^{ss} &= \frac{J_L(\epsilon)[1+n_L(\epsilon)]+J_R(\epsilon)[1+n_R(\epsilon)]}{J_L(\epsilon)[1+2n_L(\epsilon)]+J_R(\epsilon)[1+2n_R(\epsilon)]}, \\
\tilde{p}_+^{ss} &= 1-\tilde{p}_-^{ss},
\end{aligned} \tag{22}$$

with the Bose-Einstein function $n_\nu(\epsilon) = [e^{\beta_\nu \hbar\epsilon} - 1]^{-1}$. At thermal equilibrium, $T_L = T_R$, the spin occupation depends on the temperature of the bath and the spin splitting, but it does carry information on the coupling strength of the spin to the bath. In contrast, it is significant to observe signatures of the non-equilibrium situation $T_L \neq T_R$ in the levels' population, now controlled by the spectral functions of the baths. Thus, out-of-equilibrium the coupling energy to the contacts not only determines the relaxation rate towards steady-state, but it further dictates the steady-state solution. The functional form (22) has been obtained in Refs. [8, 22, 26] considering the *unbiased* spin-boson model, $\omega_0 = 0$. Thus, the seemingly more complex-biased model does not expose a nontrivial ω_0-dependent controllability.

Equations (15) and (20) complete our discussion of the RDM under the Bloch-Redfield formalism: dynamics and steady-state solution. In the next subsection we use these expressions and calculate the steady-state heat current in the NESB model.

C. Heat Current

A closed expression for quantum heat conduction in multi-state nanojunctions has been derived in Ref. [14] under a second order perturbation expansion in the system-bath coupling and the rotating wave approximation. This result was recently extended in Ref. [38] to include anti-rotating wave terms, transient effects, and lamb shifts of energies. This derivation is not repeated here; we only review its principles. Briefly, the expectation value of the heat current operator is attained from the definition (7) by time-evolving the density matrix in the energy basis to *first* order in the system-bath interaction term V_ν. The overall result is second-order in the interaction parameter since the definition of the heat current itself includes the system-bath interaction operator. We trace the current operator over the baths with a factorized system-bath initial density matrix and take the long time limit. The resulting Bloch-Redfield-type steady-state heat current formula is given by the simple form [38]

$$j_\nu = \mathrm{Tr}_S[\tilde{\rho}_S^{ss} A^\nu]. \tag{23}$$

The relevant RDM is provided in Eq. (21). The matrix A^ν depends on the properties of the subsystem; the ν index marks the terminal in which the current is calculated,

$$A^\nu_{k,j} = \sum_l S^\nu_{k,l} S^\nu_{l,j} \left(E_{l,j} w^\nu_{j\to l} + E_{l,k} (w^\nu_{k\to l})^* \right). \tag{24}$$

Here $E_{k,l} = E_k - E_l$, with the subsystem eigenenergies Eq. (10). The rate constants are given by half-range Fourier transforms of bath correlation functions,

$$\begin{aligned} w^\nu_{j\to l} &= \frac{1}{\hbar^2} \int_0^\infty d\tau e^{-iE_{l,j}\tau/\hbar} \langle B_\nu(\tau) B(0) \rangle_\nu \\ &= \frac{1}{4} \int_0^\infty d\tau e^{-iE_{l,j}\tau/\hbar} \int_0^\infty d\omega J_\nu(\omega) \left[e^{i\omega\tau} n_\nu(\omega) + e^{-i\omega\tau} (n_\nu(\omega) + 1) \right], \end{aligned} \tag{25}$$

where the real part satisfies

$$\Re[w^\nu_{j\to l}] = \frac{\pi}{4} J_\nu(|E_{l,j}|/\hbar) \times \begin{cases} n_\nu(E_{l,j}/\hbar) & \text{if } E_l > E_j \\ [n_\nu(E_{j,l}/\hbar) + 1] & \text{if } E_l < E_j. \end{cases} \tag{26}$$

Since in the energy basis the reduced density matrix of the NESB model is diagonal in steady-state, see Eq. (21), the current in Eqs. (23)-(24) immediately simplifies to

$$j_\nu = 2 \sum_{l,k} |S^\nu_{k,l}|^2 E_{l,k} (\tilde{\rho}_S^{ss})_{k,k} \Re[w^\nu_{k\to l}]. \tag{27}$$

Explicitly, for the two-state system this brings out an intuitive structure,

$$\begin{aligned} j_\nu &= 2|S^\nu_{-,+}|^2 E_{+,-} \left\{ \tilde{p}_-^{ss} \Re[w^\nu_{-\to+}] - \tilde{p}_+^{ss} \Re[w^\nu_{+\to-}] \right\} \\ &= (\hbar\epsilon) \sin^2(\theta) \Gamma_\nu(\epsilon) \left\{ \tilde{p}_-^{ss} n_\nu(\epsilon) - \tilde{p}_+^{ss} [n_\nu(\epsilon) + 1] \right\}. \end{aligned} \tag{28}$$

It describes the current, say at the L contact, by the net process of an L-bath induced excitation, multiplied by the ground state population and the energy difference $E_{+,-}$, and the relaxation from the excited state, to dispose

energy in the L bath. The second line was reached from the definition $\Gamma_\nu(\epsilon) \equiv \frac{\pi}{2} J_\nu(\epsilon)$, and by identifying the energy difference $E_{+,-} = \hbar\epsilon$. Employing the steady-state occupations (22) we obtain the closed-form result

$$j_q = (\hbar\epsilon)\sin^2(\theta)\frac{\Gamma_L(\epsilon)\Gamma_R(\epsilon)}{\Gamma_L(\epsilon)[1+2n_L(\epsilon)]+\Gamma_R(\epsilon)[1+2n_R(\epsilon)]}[n_L(\epsilon)-n_R(\epsilon)]. \tag{29}$$

The heat current can be expanded in orders of $\Delta T = T_L - T_R$ to yield the thermal conductance, a linear response coefficient (9),

$$\kappa \;=\; \sin^2\theta \frac{(\hbar\epsilon)^2}{k_B T^2}\frac{\Gamma_R(\epsilon)\Gamma_L(\epsilon)}{[\Gamma_R(\epsilon)+\Gamma_L(\epsilon)][1+2n(\epsilon)]}\frac{e^{\hbar\epsilon\beta}}{(e^{\hbar\epsilon\beta}-1)^2}. \tag{30}$$

Here $n(\omega) = [e^{\beta\hbar\omega}-1]^{-1}$ denotes the Bose-Einstein distribution function at the inverse temperature $\beta = 1/(k_B T)$. Note that $\Delta^2/\epsilon^2 = \sin^2\theta$. So far our discussion did not assume a particular spectral function. We now employ the Ohmic form (4) with a large cutoff (non-adiabatic limit), $\omega_c \gg \epsilon$, and receive [26]

$$\begin{aligned}\kappa \quad &= \quad \pi\epsilon\frac{(\hbar\Delta)^2}{k_B T^2}\frac{\alpha_L\alpha_R}{(\alpha_L+\alpha_R)}\frac{1}{2\sinh(\hbar\epsilon\beta)} \\ &\xrightarrow{\beta\hbar\epsilon\ll 1} \frac{\hbar\pi}{2}\frac{\Delta^2}{T}\frac{\alpha_L\alpha_R}{\alpha_L+\alpha_R}.\end{aligned} \tag{31}$$

In the classical high temperature limit the thermal conductance is identical for biased ($\omega_0 \neq 0$) and unbiased ($\omega_0 = 0$) models. Furthermore, the prefactor Δ^2 evinces on the expected agreement of the BR expression with the NIBA formalism for Ohmic baths, the latter technique strictly holds only in the non-adiabatic regime ($\Delta \ll \omega_c$).

IV. NONINTERACTING-BLIP APPROXIMATION: STRONG COUPLING

NIBA equations were derived for describing spin polarization dynamics in the SB model based on a path integral influence functional formalism [1, 3]. Alternatively, these equations can be recovered by transforming the SB Hamiltonian to the shifted-polaron representation, then working out a second order perturbation theory expansion of the RDM in the dressed tunneling frequency [43, 45]. NIBA serves as a good approximation for the spin polarization in the non-adiabatic limit $\omega_c >> \Delta$ [1]. For Ohmic baths, it is exact for $\langle\sigma_z(t)\rangle$ for the unbiased model at weak damping, and it can faithfully simulate the SB dynamics (polarization and coherences) at strong system-bath interactions and/or at high temperatures.

In a series of recent studies we had extended NIBA to the out-of-equilibrium regime [8, 13, 22, 23] aiming in simulating heat transport in the NESB nanojunction beyond the BR weak coupling limit. This was achieved by writing down the cumulant generating function of the system, to derive a NIBA-formula for the heat current [8, 22]. We recently proved that the approximate NIBA expression agrees with numerically-exact simulations of the thermal conductance [26] for Ohmic reservoirs, working in the high temperature limit.

In Sec. IV A we include equations of motion for the spin RDM under NIBA [1]. The NIBA heat current expression was first constructed in Ref. [8]; it was later formally derived from a counting-statistics approach in Ref. [22]. In Sec. IV B we include relevant expressions.

A. Reduced density matrix

The exact-formal series expansion of $\langle\sigma_z(t)\rangle$ in Δ can be organized as a generalized master equation. The dynamics of off-diagonal terms $\langle\sigma_{x,y}(t)\rangle$ is obtained from the polarization $\langle\sigma_z(t)\rangle$ by exact integral relations [1],

$$\begin{aligned}\frac{d\langle\sigma_z\rangle}{dt} \;&=\; -\int_0^t K_{s,z}(t-\tau)\langle\sigma_z(\tau)\rangle d\tau - \int_0^t K_{a,z}(t-\tau)d\tau, \\ \langle\sigma_x\rangle \;&=\; \int_0^t K_{s,x}(t-\tau)d\tau - \int_0^t K_{a,x}(t-\tau)\langle\sigma_z(\tau)\rangle d\tau, \\ \langle\sigma_y\rangle \;&=\; \frac{1}{\Delta}\frac{d\langle\sigma_z\rangle}{dt}.\end{aligned} \tag{32}$$

The (exact) kernels in Eq. (32) can be truncated to include lowest-nontrivial terms in Δ. This scheme, termed the noninteracting-blip approximation, results in [1],

$$\begin{aligned} K_{s,z}(t) &= \Delta^2 e^{-Q'(t)}\cos[Q''(t)]\cos(\omega_0 t), \\ K_{a,z}(t) &= \Delta^2 e^{-Q'(t)}\sin[Q''(t)]\sin(\omega_0 t), \\ K_{s,x}(t) &= \Delta e^{-Q'(t)}\cos[Q''(t)]\sin(\omega_0 t), \\ K_{a,x}(t) &= \Delta e^{-Q'(t)}\sin[Q''(t)]\cos(\omega_0 t). \end{aligned} \tag{33}$$

The function $Q(t)=\sum_\nu Q_\nu(t)$, $Q_\nu(t)=Q'_\nu(t)+iQ''_\nu(t)$ contains real and imaginary components with

$$\begin{aligned} Q'_\nu(t) &= \int_0^\infty d\omega \frac{J_\nu(\omega)}{\omega^2}[1-\cos(\omega t)][1+2n_\nu(\omega)], \\ Q''_\nu(t) &= \int_0^\infty d\omega \frac{J_\nu(\omega)}{\omega^2}\sin(\omega t). \end{aligned} \tag{34}$$

In an equilibrium situation, $T_L=T_R$, $\langle\sigma_x\rangle_{eq}=-\frac{\Delta}{\omega_0}\tanh\left(\frac{\beta\hbar\omega_0}{2}\right)$ and $\langle\sigma_z\rangle_{eq}=-\tanh\left(\frac{\beta\hbar\omega_0}{2}\right)$ [3]. The out-of-equilibrium steady-state solution of the Markovian equation satisfies [8, 22]

$$\langle\sigma_z\rangle_{ss}=[k(-\omega_0)-k(\omega_0)]/[k(-\omega_0)+k(\omega_0)], \tag{35}$$

where the rates are convolutions of the L and R baths-induced rates,

$$\begin{aligned} k(\omega_0) &= \int_{-\infty}^\infty e^{i\omega_0 t}e^{-Q_L(t)}e^{-Q_R(t)}dt \\ &= \frac{1}{2\pi}\int_{-\infty}^\infty k_L(\omega_0-\omega)k_R(\omega)d\omega. \end{aligned} \tag{36}$$

The "Fermi-Golden-Rule" rate constant $k_\nu(\omega)$ ($\times\Delta^2$) was originally derived in the context of reaction rates in donor-acceptor complexes [2],

$$k_\nu(\omega)=\int_{-\infty}^\infty e^{i\omega t}e^{-Q_\nu(t)}dt, \tag{37}$$

and it satisfies the detailed balance relation,

$$k_\nu(-\omega)=k_\nu(\omega)e^{-\beta\hbar\omega}. \tag{38}$$

In the Ohmic case, in the scaling regime, $k_BT,\hbar\omega<\hbar\omega_c$, the ν-bath-induced rate obeys [1]

$$k_\nu(\omega)=\frac{1}{\omega_c}\left(\frac{\hbar\omega_c}{2\pi k_BT}\right)^{1-2\alpha_\nu}\frac{|\Gamma(\alpha_\nu+i\hbar\omega/2\pi k_BT)|^2}{\Gamma(2\alpha_\nu)}e^{\hbar\omega/2k_BT}. \tag{39}$$

Closed expressions for $k(\omega)$, thus the polarization, are missing in general since the convolution (36) is nontrivial to handle analytically. As we show below, NIBA heat current relies on the steady-state population of the spin states (in the local basis), $p_1^{ss}=(1+\langle\sigma_z\rangle_{ss})/2$, $p_0=1-p_1$, but it does not contain the coherences. In equilibrium, the spin occupation obeys

$$p_1^{eq}=\frac{e^{-\beta\hbar\omega_0/2}}{e^{-\beta\hbar\omega_0/2}+e^{\beta\hbar\omega_0/2}}. \tag{40}$$

It is of interest to acquire $p_{1,0}^{ss}$ approximately-analytically, to study signatures of the non-equilibrium condition on the TLS at strong system-bath couplings.

B. Heat current

A closed expression for the steady-state heat current under NIBA has been derived by energy-unraveling the polarization dynamics, Eq. (32) [22], resulting in

$$j_q=\left(\frac{\Delta}{2}\right)^2\frac{\hbar}{2\pi}\int_{-\infty}^\infty \omega d\omega\left[k_R(\omega)k_L(\omega_0-\omega)p_1^{ss}-k_R(-\omega)k_L(-\omega_0+\omega)p_0^{ss}\right]. \tag{41}$$

Considering the unbiased model, the thermal conductance is given by the compact form [23]

$$\kappa = \left(\frac{\Delta}{2}\right)^2 \frac{\hbar^2}{4\pi k_B T^2} \int_{-\infty}^{\infty} \omega^2 k_R(\omega) k_L(-\omega) d\omega. \tag{42}$$

In the high T limit we substitute Eq. (39) into Eq. (42) and receive [23]

$$\begin{aligned} \kappa &\simeq \mathcal{A}\hbar^2 \left(\frac{\Delta}{\omega_c}\right)^2 \frac{1}{k_B T^2} \left(\frac{\hbar\omega_c}{k_B T}\right)^{2-2\alpha_L-2\alpha_R} \int_0^{k_B T/\hbar} \omega^2 d\omega \\ &\simeq \mathcal{A}\frac{k_B \Delta^2}{\omega_c} \left(\frac{\hbar\omega_c}{k_B T}\right)^{1-2\alpha}. \end{aligned} \tag{43}$$

We emphasize that under NIBA the heat current, Eq. (41), is only determined by the polarization dynamics and its decay rates to steady-state. This observation explains the satisfactory performance of NIBA (with α) in heat transfer calculations [23]: NIBA truncation of $K_{s/a,z}$ carries errors (in the inter-blip correlations of the kernel) only second-order in α. As a result, the dynamics of $\langle\sigma_z(t)\rangle$ is exact for the unbiased and weakly-damped NESB model. In contrast, the kernels $K_{s/a,x}$ carry first-order errors in α, making them inaccurate even for the unbiased SB model. However, these errors do not propagate into the NIBA heat current formula.

V. PATH INTEGRAL SIMULATIONS: QUAPI AND INFPI

The numerically exact iterative quasi-adiabatic path-integral (QUAPI) approach has been developed by Makri and Makarov for simulating the reduced spin dynamics in the spin-boson model [47]. It allows one to treat strong system-bath couplings and to include non-Markovian effects. Recent efforts directed excitonic energy transfer in biomolecules, treating more complex situations, considering (a single excitation in) multiple sites and prominent vibrations in each site [48].

The QUAPI algorithm had been constructed on the grounds of harmonic environments linearly coupled to the subsystem [47]. In this situation, the effect of the environment on the subsystem's RDM can be absorbed in an analytic function, the "Feynman-Vernon influence functional" [49]. At nonzero temperatures the memory function within the influence functional decays rapidly in time, allowing for its controlled truncation and the development of an iterative time evolution scheme [47].

This principle can be generalized to construct a QUAPI-type algorithm for anharmonic baths [50]. Furthermore, a related-general approach, the so-called "influence functional path integral" (INFPI) tool has been put forward for treating quantum systems in contact with multiple fermionic reservoirs at finite bias voltages [51]. This approach can be excersized when an exact analytic form for the influence functional is missing, as it is computed numerically using trace identities. Given their conceptual similarity, QUAPI and INFPI were recently combined for a unified study of charge transport and vibrational excitation and dissipation in donor-acceptor molecular electronic diodes [52].

The standard QUAPI algorithm administers only the dynamics of the reduced density matrix [47]. The calculation of other observables, particularly the heat current in the NESB model, necessitates significant technical advances. In contrast, the INFPI algorithm has been formulated for treating a generic impurity Hamiltonian [51, 52] and with little effort it can be employed for the study of other observables of quadratic structure, beyond the RDM. For example, INFPI has been applied for the investigation of charge current [51] and equilibration dynamics [53] in the single-impurity Anderson model, More recently, we adopted INFPI to simulate qubit-mediated energy flow between metals [25].

Algorithmic details of QUAPI [47] and INFPI [51, 52] can be found elsewhere. Here we only highlight their working principles and associated numerical errors. The starting point of these techniques involves the Trotter factorization of the time evolution operator, e.g., into a free subsystem term and bath-related propagators. After collecting the environmental contributions and tracing over the baths we reach an influence functional-type expression, see Eq. (44) below. As mentioned above, at finite temperatures and/or a nonzero chemical potential bias bath correlations exponentially decay in time [54–56], allowing for their truncation beyond a memory time τ_c. An iterative time evolution scheme can then be constructed by defining an auxiliary quantity (an extension of the observable of interest) on the time-window τ_c. This time-nonlocal object can be iteratively evolved from the initial condition to the final time t.

Simulations with QUAPI and INFPI involve two numerical errors: (i) Trotter error due to the finite time-step adopted in the Trotter breakup δt, and (ii) an error associated with the truncation of the influence functional to cover a certain time window τ_c. Furthermore, in INFPI the Fermi sea is discretized. Thus, one should confirm that within the relevant simulation time the number of bath states does not affect results.

A. Reduced density matrix

The original QUAPI algorithm provided the subsystem's RDM when coupled to a single harmonic bath. Here QUAPI is (trivially) extended to accommodate two reservoirs of different temperatures. The time evolution of the RDM up to $t = N\delta t$, N is an integer, can be represented in a path integral formulation as [47],

$$\langle s_N^+|\rho_S(t)|s_N^-\rangle = \int ds_0^\pm \int ds_1^\pm ... \int ds_{N-1}^\pm I^{har}(s_0^\pm, s_1^\pm, ..., s_N^\pm). \tag{44}$$

Here $s_k^\pm$ represent the discrete path of the subsystem on the forward (+) and backward (−) contours (not to be confused with the eigenstates of H_S described in Sec. III A). As an initial condition we assume that $\rho(0) = \rho_L \otimes \rho_R \otimes \rho_S(0)$ with the baths separated from the subsystem. The integrand in Eq. (44) is refereed to as an "Influence Functional" (IF) [49]; note that in Refs. [47, 49] it was identified without the free-subsystem evolution terms. For a harmonic bath bilinearly coupled to the subsystem the IF is given by an exponential of a quadratic structure, multiplied by free subsystem propagation terms,

$$\begin{aligned} I^{har}(s_0^\pm, ..., s_N^\pm) &= \exp\Big[-\sum_\nu \sum_k^N \sum_{k'=0}^k (s_k^+ - s_k^-)(\eta_{k,k'}^\nu s_{k'}^+ - \eta_{k,k'}^{\nu *} s_{k'}^-)\Big] \\ &\times \langle s_N^+|e^{-iH_0\delta t}|s_{N-1}^+\rangle ... \langle s_0^+|\rho_S(0)|s_0^-\rangle ... \langle s_{N-1}^-|e^{iH_0\delta t}|s_N^-\rangle. \end{aligned} \tag{45}$$

The free Hamiltonian H_0 is defined in Eq. (1), the coefficients $\eta_{k,k'}^\nu$ depend on the spectral function of the ν bath and its temperature. They were derived in Ref. [47] by discretizing the Feynman-Vernon IF.

B. Heat Current

The heat current in the NESB model can be written as a Meir-Wingreen formula combining spin-spin correlation functions [18]. Here, rather than generalizing QUAPI to follow correlation functions in a non-equilibrium setup, a nontrivial task, we study the behavior of the NESB model through the related fermionic model, naturally handled by INFPI.

The spin-boson Hamiltonian can be reached by bosonizing the spin-fermion (SF) model, comprising a spin [Eq. (1)] and two metallic leads $\nu = L, R$, 1D electron gases with linear dispersion. The metals are prepared at different temperatures but at the same chemical potential. They are connected indirectly, only through the TLS, blocking charge transfer between the metals but allowing for energy flow. The total non-equilibrium spin-fermion (NESF) Hamiltonian reads

$$H_{SF} = H_0 + \hbar\sigma_z \sum_{\nu,p,p'} g_{p,\nu;p',\nu} c_{p,\nu}^\dagger c_{p',\nu} + \sum_{\nu,p} \epsilon_{p,\nu} c_{p,\nu}^\dagger c_{p,\nu}. \tag{46}$$

Here $c_{p,\nu}^\dagger$ ($c_{p,\nu}$) represents a fermionic creation (annihilation) operator. The spin polarization couples to intra-bath electron-hole pair generation as in Ref. [25]. The coupling parameter $g_{p,\nu;p',\nu}$ (taken as a constant g_ν in simulations) relates the NESB model to the boson picture via the relation [3]

$$\alpha_\nu = \frac{1}{2}\left[\frac{2}{\pi}\mathrm{atan}(\pi\rho_\nu(\epsilon_F)g_\nu)\right]^2. \tag{47}$$

Here $\rho_\nu(\epsilon_F)$ is the density of states at the Fermi energy and α_ν is a dimensionless parameter, the prefactor in the bosonic-Ohmic spectral function, see Eq. (4).

We had recently simulated the energy current characteristics of the unbiased NESF model by adapting the INFPI approach [25]. We discuss next the structure of the current operator in this simulation. First, we transform the Hamiltonian (46) via a unitary transformation $\tilde{H}_{SF} = U^\dagger H_{SF} U$ as in Sec. III A into

$$\tilde{H}_{SF} = H_S + H_F + V, \tag{48}$$

where

$$\begin{aligned} H_S &= \frac{\hbar\epsilon}{2}\tilde{\sigma}_z, \\ H_F &= H_L + H_R, \quad H_\nu = \sum_p \epsilon_p c_{p,\nu}^\dagger c_{p,\nu}, \\ V &= V_L + V_R, \quad V_\nu = \tilde{\sigma}_x \sum_{p,p'} \hbar g_{p,\nu;p'\nu} c_{p,\nu}^\dagger c_{p',\nu} \end{aligned} \tag{49}$$

As before, $\tilde{\sigma}_{x,y,z}$ stand for Pauli matrices in the energy basis. We assume a factorized initial state, $\tilde{\rho}(0) = \tilde{\rho}_S(0) \otimes \rho_L \otimes \rho_R$, $\tilde{\rho}_S$ denotes the reduced density matrix of the subsystem and $\rho_\nu = e^{-\beta_\nu(H_\nu - \mu_\nu N_\nu)}/\mathrm{Tr}_\nu[e^{-\beta_\nu(H_\nu-\mu_\nu N_\nu)}]$. In our simulations below we take $\mu_L = \mu_R$ but assume different (time-zero) temperatures for the thermal baths, $T_L \neq T_R$. At $t = 0$ we put into contact the two Fermi baths through the quantum subsystem, then follow the evolution of the reduced density matrix and the energy current until (quasi) steady-state sets in. Since electron flow is blocked and energy is transferred through excitation - de-excitation processes of the TLS, we refer to the energy current here as a "heat current".

The heat current in the unbiased ($\omega_0 = 0$) model was calculated in the energy basis using the construction [14]

$$j_L = \mathrm{Tr}_S \mathrm{Tr}_F[\tilde{\dot{j}}_L \rho(t)] = -\frac{i}{\hbar}\mathrm{Tr}_S \mathrm{Tr}_F\{\tilde{\rho}(t)[H_S, V_L]\}, \tag{50}$$

obtained from the definition (7) under a steady-state assumption. Here, Tr_F (Tr_S) refers to a partial trace over the Fermi-sea electrons (TLS). We identify the current with the contact at which it is evaluated, though $j_q = j_L = -j_R$ is satisfied here. The commutator can be readily performed to yield

$$[H_S, V_L] = i\hbar^2 \Delta \tilde{\sigma}_y \sum_{l,l'} g_{l,L;l',L} c^\dagger_{l,L} c_{l',L}, \tag{51}$$

leading to

$$j_L = (\hbar\Delta)\mathrm{Tr}_S\left[\tilde{\sigma}_y \mathrm{Tr}_\mathrm{F}[A_L \tilde{\rho}(t)]\right]. \tag{52}$$

The bath operator is given by $A_L \equiv \sum_{l,l'} g_{l,L;l',L} c^\dagger_{l,L} c_{l',L}$. We now further define a subsystem operator as

$$A_S(t) \equiv \mathrm{Tr}_\mathrm{F}[A_L \rho(t)] = \mathrm{Tr}_\mathrm{F}[e^{iHt/\hbar} A_L e^{-iHt/\hbar} \tilde{\rho}(0)], \tag{53}$$

and express the current with its matrix elements

$$j_L = (\hbar\Delta)[-i(A_S(t))_{-,+} + i(A_S(t))_{+,-}]. \tag{54}$$

We use INFPI to time-evolve Eq. (53) [25]. These Simulations are compared to BR and NIBA results from Secs. III C and IV B, respectively.

VI. SIMULATIONS

The dynamics of the reduced density matrix is obtained by solving numerically the BR and NIBA integro-differential equations, Eq. (15) and (32), respectively, using the trapezoidal rule for the inner integral, see Ref. [46]. This brute-force approach was adopted with a small time step, $\delta t = T_p/2000$; the period is defined by $T_p \equiv 2\pi/\epsilon$. Integrals over frequency were evaluated using the trapezoidal rule, discretized with $\delta\omega \sim \epsilon/2000$, up to the limit $30\omega_c$. QUAPI and INFPI simulations were performed with $\delta t \sim T_p/50$. Other parameters are $k_B T/\hbar\Delta \sim 1-2$, $\omega_0/\Delta = 0-5$, $\omega_c = 20\Delta$ and $\alpha_\nu = 10^{-3}-1$. Thermal conductances were calculated by taking a small temperature difference, $2(T_L - T_R)/[(T_L + T_R)] = 0.05$. INFPI simulations better converge for larger temperature differences, $k_B(T_L - T_R)/\hbar\Delta \sim 1$. We use here an Ohmic spectral function, but we are not limited to this form and other environments can be similarly explored, e.g., a Debye spectral function or a spin bath mimicked by a harmonic environment, with a temperature-dependent spectral function [57].

A. Unbiased model

RDM Dynamics. We begin with the unbiased $\omega_0 = 0$ model. In Figs. 2-4 we follow the dynamics of the subsystem in the local basis ($|0\rangle$, $|1\rangle$) using BR, NIBA and QUAPI [47], extended here to the non-equilibrium two-bath case. At very weak coupling, $\alpha_\nu = 0.025$, BR and NIBA reasonably agree with QUAPI; at smaller couplings, $\alpha < 0.02$, the agreement is excellent (not shown). Increasing the coupling to $\alpha = 0.1 - 0.15$, translating to a total interaction strength $\alpha = 0.2 - 0.3$, we note that NIBA and BR agree with QUAPI over the polarization dynamics, but the real part of off-diagonal elements deviate up to a factor of 1.5 in the steady-state limit.

Heat transfer: Coupling to the contacts. Deviations between BR and NIBA in the RDM behavior propagate into significant, qualitative differences in the heat current characteristics. In Fig. 5 we display the thermal conductance of

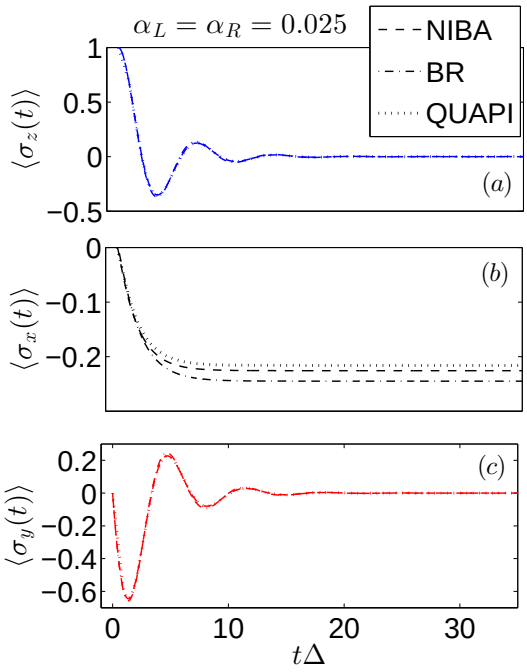

FIG. 2: Dynamics of the spin subsystem in the NESB model assuming an Ohmic spectral function with $\omega_c = 20\Delta$, and $k_BT_L = k_BT_R = 2\hbar\Delta$, $\omega_0 = 0$, $\alpha_L = \alpha_R = 0.025$. (a-c) Results for $\langle\sigma_{x,y,z}(t)\rangle$ are presented in the local basis ($|0\rangle$ and $|1\rangle$), QUAPI (dotted), NIBA (dashed), BR (dashed-dotted).

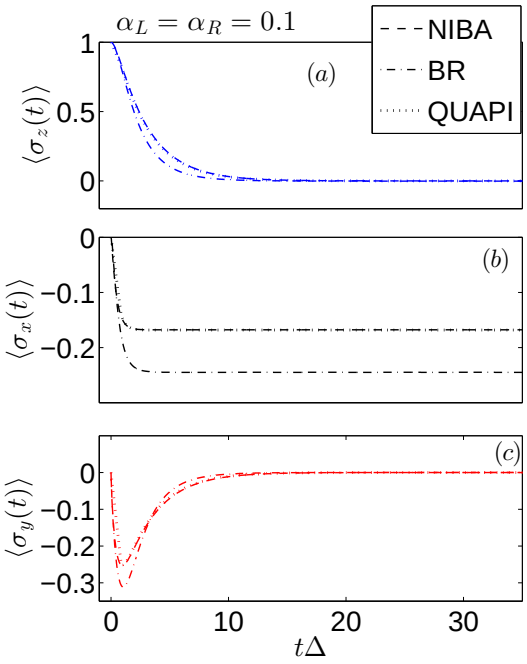

FIG. 3: Dynamics of the spin subsystem with the parameters of Fig. 2, $\alpha_L = \alpha_R = 0.1$.

the NESB model and show that within the BR scheme it grows linearly with α [8], while NIBA demonstrates saturation of the current, then its decay at large values of α [23]. We also illustrate the behavior of the thermal conductance using the NEGF-Redfield scheme of Ref. [18]. In this approach correlation functions in the (exact) heat transfer Meir-Wingreen formula are evaluated at the level of the Redfield theory, which is second order in the system-bath coupling. A different NEGF-based expression for the heat current was proposed in Ref. [21]. It was obtained from the diagrammatic expansion, by calculating the spin-spin correlation functions via the Majorana-fermion representation

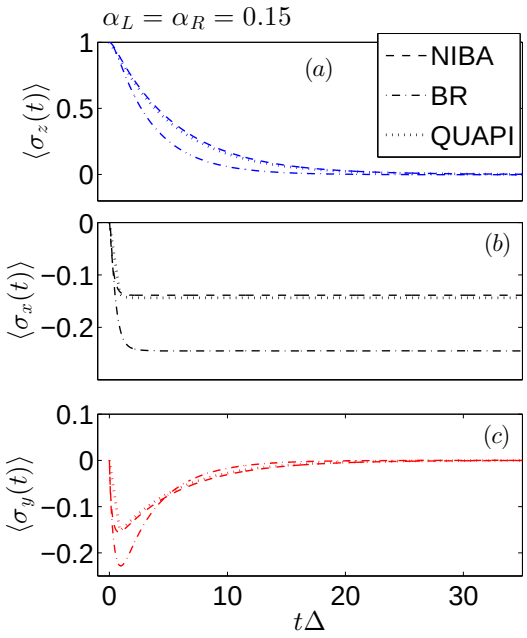

FIG. 4: Dynamics of the spin subsystem as in Fig. 2, with $\alpha_L = \alpha_R = 0.15$.

of spin operators, truncating diagrams of high order system-bath couplings. This results in an elegant expression (presented here for $\omega_0 = 0$),

$$j_q = \frac{2}{\pi}\int_0^\infty \frac{\hbar\omega\Delta^2\Gamma_R(\omega)\Gamma_L(\omega)}{(\omega^2-\Delta^2)^2 + [\Gamma_L(\omega)\coth(\beta_L\hbar\omega/2) + \Gamma_R(\omega)\coth(\beta_R\hbar\omega/2)]^2\omega^2)}[n_L(\omega) - n_R(\omega)]d\omega. \tag{55}$$

This formula resembles the harmonic limit [58], and it nicely interpolates between the very weak coupling equation (29), resulting from a kinetic-type dynamics, and the low-temperature limit, where heat is transferred coherently, out of resonance with the central frequency; the integration over frequencies away from Δ reflects a tunneling behavior.

We see in Fig. 5 that the two NEGF-based approaches perform very well up to $\alpha_\nu = 0.1$. Predictions beyond that are qualitatively incorrect as these methods fail to provide the decay behavior of the current with α at strong coupling. However, even in this regime NEGF-Redfield and the NEGF expression (55) are valuable tools; their predictions are significantly closer to NIBA than to BR.

In Fig. 6 we use INFPI to simulate the heat current in the NESF model [25]. We display the current as a function of the interaction parameter α up to $\alpha/2 = 0.1$, which we consider as a weak-intermediate value. We compare INFPI results to the predictions of BR, NIBA, NEGF-Redfield [18] and NEGF of Ref. [21]. BR equation fails beyond $\alpha/2 = 0.02$, but the other methods excellently agree. Note that in the fermionic language $\alpha/2 = 0.1$ translates to a phase shift of $\phi_\nu = \pi\rho_\nu\alpha_\nu \sim 1$. It is useful to comment at this point that a fully harmonic junction is expected to provide higher currents than supported by the (anharmonic) NESB junction [58]. Specifically, under a weak coupling approximation the current in harmonic junctions obeys Eq. (29), only missing the temperature-dependent distribution functions in the denominator.

We now explain our classification of system-bath coupling domains based on Figs. 5-6. In the very weak coupling limit $\alpha_\nu < 0.025$ the Bloch-Redfield treatment is valid within up to 10% deviations from exact results. In the so-called weak coupling regime $0.025 < \alpha_\nu < 0.1$ deviations from linearity are apparent, but the current is growing monotonically with α. For stronger couplings, $0.1 < \alpha_\nu < 0.5$, the heat current displays a crossover behavior: Fig. 5 shows that beyond $\alpha_\nu = 0.15$ the thermal conductance drops with increasing couplings to the bath. We refer to this crossover area as the intermediate coupling regime. At even stronger coupling the behavior of $j_q(\alpha)$, or the thermal conductance, is dominated by an exponentially decaying factor of α, see Eq. (43).

Beyond the non-adiabatic limit. The non-adiabatic limit describes a junction comprising a low-frequency (slow) central vibration, relative to the cutoff frequency of the bath. In Fig. 7 we abandon the strict non-adiabatic region and explore the dynamics when $\Delta/\omega_c = 0.25$ with $2.5k_BT_\nu = \hbar\Delta$. We study the time evolution of the RDM at very weak coupling and find that NIBA fails to reproduce $\langle\sigma_x(t)\rangle$, deviating by $\sim 40\%$, while it performs well for the polarization dynamics. We now discuss implications on transport properties.

The effect of the spin tunneling frequency Δ on the steady-state heat current is displayed in Fig. 8, considering

a weakly coupled nanojunction. The heat current exhibits a turnover behavior as a function of Δ, explained based on the BR expression (29): The current increases with Δ, the quanta transmitted, but it further requires a sufficient thermal occupation factor in matching bath modes. Thus, when the tunneling frequency is high, $\Delta > 2k_BT/\hbar$, the current begins to drop due to reduced population of in-resonance modes. Comparing BR (dashed) to INFPI (square), we find that the BR scheme reproduces the correct turnover behavior, though the exact position of the maxima is shifted, and the magnitude of the current is overestimated at high temperatures [60]. NEGF results are not displayed here; in this weak-coupling regime they overlap with BR. In contrast, NIBA equations miss altogether the correct behavior of $j_q(\Delta)$ once $\Delta/\omega_c > 0.1$ since NIBA only captures non-adiabatic contributions, $j_q \propto \Delta^2$. Moreover, it is interesting to note that not only does NIBA provide the wrong functional form for $j_q(\Delta)$, it further predicts an erroneous temperature-dependent behavior: While in the non-adiabatic regime at small coupling the current drops with increasing temperatures, $j_q \propto T^{-1}$, a tendency captured by NIBA, the opposite behavior takes place beyond the non-adiabatic regime once the current is controlled by thermal occupation factors in the contacts.

Another interesting observation concerns the low temperature $k_BT_a/\hbar\omega_c = 0.07$ regime, see Fig. 8(c). In this case INFPI simulations indicate on the existence of *two* peaks in the current $j_q(\Delta)$, at Δ/ω_c=0.25, 0.65. The first peak corresponds to absorption and emission processes of a single phonon in either the L or R baths, as explained above. In the language of the SF model, these are single electron-hole pair generation or destruction processes. Around Δ/ω_c=0.25, the enhancement of the current with an enlarging spin frequency is balanced by thermal occupation factors of bath modes. We presume that the second peak corresponds to a similar balance, apparently reflecting two-phonon processes (two electron-hole pairs) participating in the excitation and relaxation dynamics of the TLS. Additional simulations are required to establish this result.

Heat transfer: Temperature dependence. The temperature dependence of the thermal conductance is of particular interest for actual devices; exact Monte-Carlo simulations [26] provided the high temperature behavior of the NESB model $\kappa \propto \left(\frac{k_BT}{\hbar\omega_c}\right)^{2\alpha-1}$ and the low-temperature scaling $\kappa \propto \alpha(T/T_K)^3$, T_K is the Kondo temperature in the system, a function of the microscopic parameters Δ, ω_c and α. We had recently proved that the high-temperature limit is reproduced by NIBA-heat current formula, see Eq. (43) [23]. Fig. 9 displays the thermal conductance characteristics with temperature in the non-adiabatic limit at intermediate and weak (inset) coupling. In the weak coupling limit the three techniques coincide at high temperatures. In contrast, at stronger coupling the (correct) NIBA scaling is neither reproduced by BR nor by NEGF. It is also significant to comment that NIBA misses altogether the enhancement of the conductance with T for $k_BT_a/\hbar\Delta < 0.5$. Therefore, it is crucial to carefully examine parameters of interest to determine which technique is most suitable.

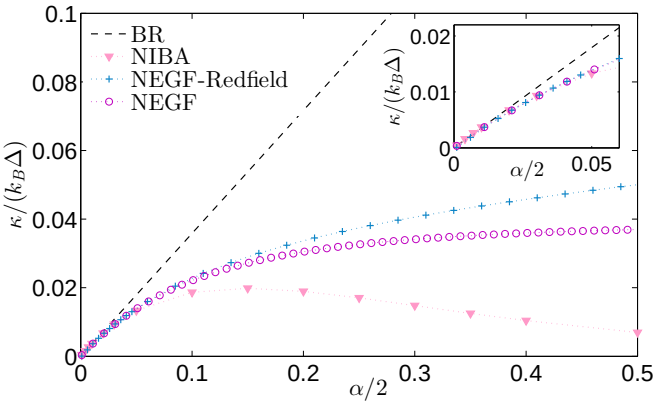

FIG. 5: Thermal conductance in the unbiased NESB model as a function of $\alpha/2 = \alpha_L = \alpha_R$. We use Ohmic spectral functions with $\omega_c = 20\Delta$, $\omega_0 = 0$, $k_BT_L = 2.05\hbar\Delta$, $k_BT_R = 1.95\hbar\Delta$ with BR (dashed), NIBA ($\triangledown$), NEGF-Redfield from Ref. [18] (+) and the NEGF expression (55) from Ref. [21] ($\circ$). The inset zooms over the weak coupling regime.

B. Biased model

RDM dynamics. In Fig. 10 we display the RDM dynamics in the biased model. At weak coupling NIBA misses the correct behavior of the RDM [1] while at strong coupling it reasonably agrees with QUAPI.

Thermal conductance. Since the NIBA-heat current expression only depends on the polarization dynamics (steady-state value and the relaxation rates), errors in $\langle\sigma_x(t)\rangle$ do not propagate into the calculation of the heat current, see

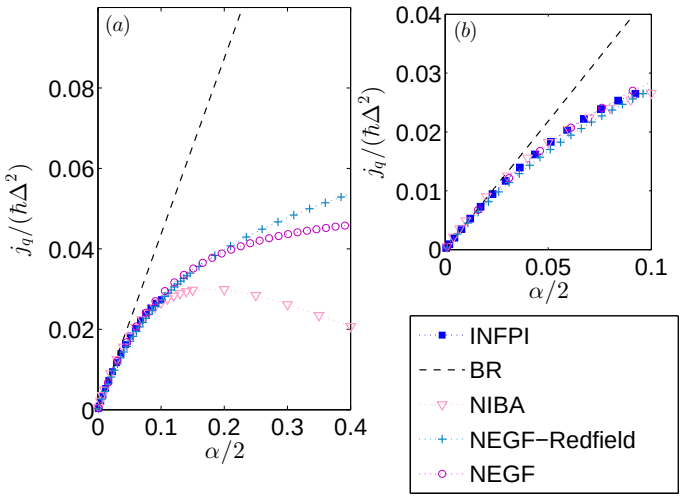

FIG. 6: (a) Heat current in the unbiased NESF model. Simulations were performed in the fermionic picture using electron bands with linear dispersion and a hard cutoff at $D/\Delta = \pm 5$. The parameters of the fermionic model are matched with the bosonic picture using Eq. (47), $\alpha_L = \alpha_R$, $\omega_0 = 0$, $k_BT_L = 2\hbar\Delta$, $k_BT_R = \hbar\Delta$. We compare INFPI (□) to simulations in the bosonic picture, BR (dashed), NIBA (▽), NEGF-Redfield [18] (+) and the NEGF expression (55) [21] (○). Panel (b) zooms over the small-α regime. INFPI numerical parameters are $\delta t = 0.1/\Delta$ and $N_s = 9$, for more details see Ref. [25].

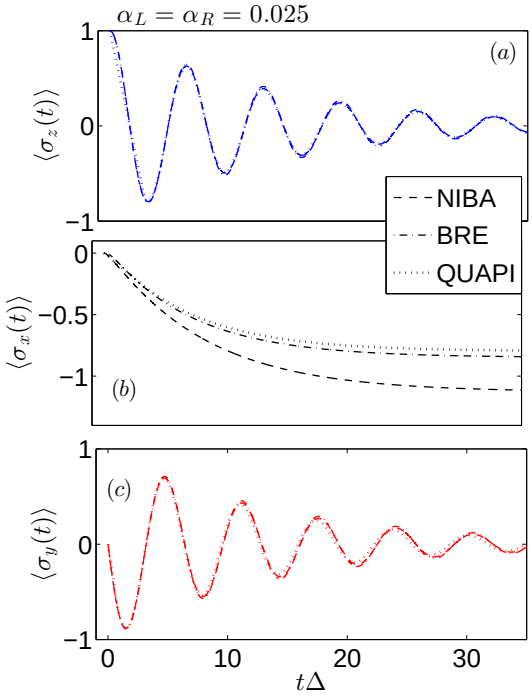

FIG. 7: Dynamics of the unbiased model beyond the non-adiabatic region for $\omega_c = 4\Delta$, $k_BT_L = k_BT_R = \hbar\Delta/2.5$, and $\alpha_L = \alpha_R = 0.025$. QUAPI (dotted), NIBA (dashed), BR (dashed-dotted).

Fig. 11. The bias affects the conductance in a simple way: In the BR scheme $\kappa \propto \epsilon/\sinh(\beta\hbar\epsilon)$, see Eq. (31). In NIBA calculations we confirmed numerically that $\kappa \propto \omega_0/\sinh(\beta\hbar\omega_0)$, for $\alpha = 0.1 - 0.5$. Thus, the bias does not offer a new "quantum" control knob over the heat current as ω_0 does not tangle with the coupling strength α in the present non-adiabatic limit.

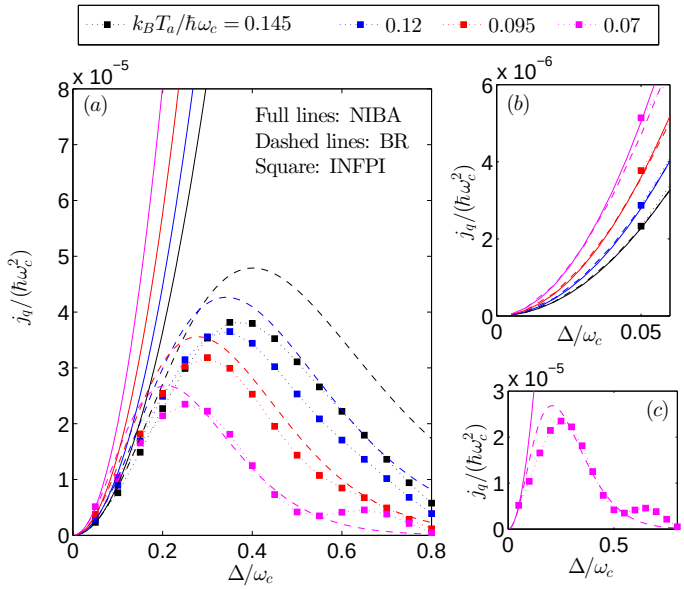

FIG. 8: Heat current as a function of the TLS tunneling frequency. (a) INFPI simulations in the fermionic picture (□). The parameters of the fermionic model are matched with the bosonic case using Eq. (47), $\pi\rho(\epsilon_F)g = 0.3$, leading to $\alpha_L = \alpha_R = 0.0172$. Other parameters are $\omega_0 = 0$, $k_BT_a/\hbar\omega_c$ as indicated in the legend with $T_a = (T_L + T_R)/2$ and $(T_L - T_R)/\omega_c = 0.01$. We compare INFPI (□) results to simulations in the bosonic picture, BR (dashed), NIBA (full). Panel (b) zooms over the non-adiabatic regime. INFPI numerical parameters are $\delta t = 0.1/\Delta$ and $N_s = 9$, for more details see Ref. [25]. Panel (c) zooms over the low temperature case, $k_BT_a/\hbar\omega_c = 0.07$.

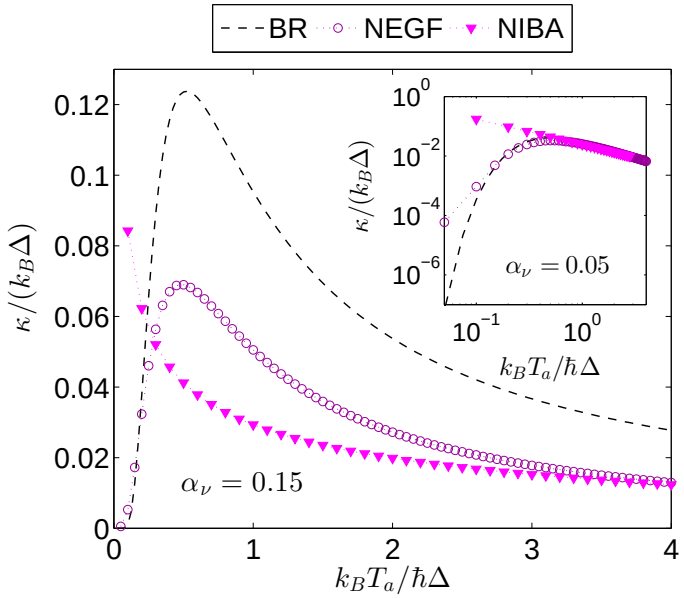

FIG. 9: Thermal conductance in the unbiased NESB model as a function of temperature. We use Ohmic spectral functions with $\omega_c = 20\Delta$, $\alpha_\nu = 0.15$. BR (dashed), NIBA (▽), and the NEGF expression (55) [21] (○). NEGF-Redfield formula did not provide physical answers at high temperatures here. The inset displays a weak coupling example with $\alpha_\nu = 0.05$.

VII. SUMMARY

We provided a comprehensive analysis of the non-equilibrium spin-boson model, comprising a spin subsystem coupled to two thermal baths of different temperatures. We studied the dynamics of the spin reduced density matrix and the transfer of heat in the model using different techniques: the Bloch-Redfield scheme which is valid in the very weak system-bath coupling limit, the noninteracting-blip approximation, exact in the non-adiabatic ($\Delta \ll \omega_c$) scaling

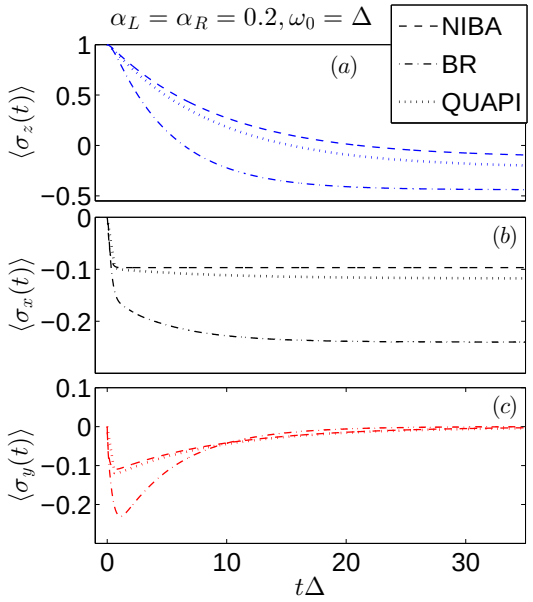

FIG. 10: Dynamics of the biased model $\omega_0 = \Delta$ in the intermediate coupling regime, $\alpha_L = \alpha_R = 0.2$, and $\omega_c = 20\Delta$, $k_B T_L = k_B T_R = 2\hbar\Delta$. QUAPI (dotted), NIBA (dashed), BR (dashed-dotted).

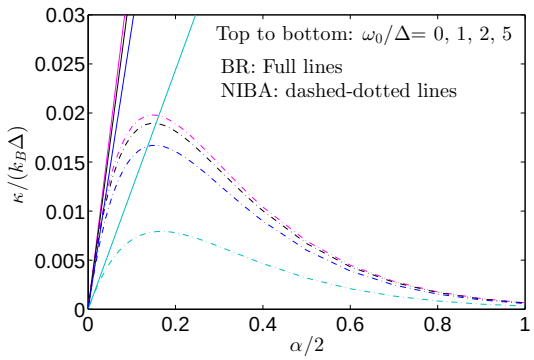

FIG. 11: Thermal conductance for the biased model assuming Ohmic spectral functions and $\alpha_L = \alpha_R$, $\omega_c = 20\Delta$, $k_B T_L = 2.05\hbar\Delta$, $k_B T_R = 1.95\hbar\Delta$.

limit, and numerically-exact influence functional path integral simulations. We also compared results to NEGF-based techniques [18, 21]. The BR, NIBA and path integral approaches were originally developed for exploring decoherence effects and dissipation in open quantum systems. Here we bring an organized discussion of their extensions to treat transport behavior.

Specific observations include: (i) The biased and unbiased NESB models may display similar dynamics within the BR and NIBA approaches, but relatively small deviations in the RDM behavior propagate into strong and qualitative disagreements in the heat current characteristics. (ii) The BR formalism should be used with great caution in modeling actual devices since the prediction $j_q \propto \alpha$ fails beyond the very weak coupling limit, providing unphysical-incorrect large conductances. (iii) In the regime of validity for BR and NIBA, the spin bias (detuning) parameter does not offer a new-nontrivial control mean over the heat current; at large detuning the current decays since thermal occupation of high frequency bath modes (above the thermal energy) is reduced. (iv) In the non-adiabatic regime at weak coupling and high temperatures, the thermal conductance decreases with increasing temperatures, $\kappa \propto (T_L - T_R)/T$. This behavior stems from the intrinsic anharmonicity of the junction. This trend is correctly captured by the BR method, NIBA and INFPI. In contrast, beyond the non-adiabatic limit this trend is reversed since thermal occupation factors of bath modes dominate the current rather than temperature-dependent (anharmonic) scatterings in the junction. As expected, NIBA fails to capture this behavior: It overestimates the current by orders of magnitude and it predicts an enhancement of the current when reducing the temperature, irrespective of the frequency Δ.

It is of interest to extend our analysis and further explore the behavior under classical equations of motion, or

mixed quantum-classical treatments [61]. Future studies will also examine the time-dependent-driven NESB model [62–65] with the objective to understand the role of strong system-bath couplings and quantum coherence in possibly enhancing heat to work conversion efficiency.

Acknowledgments

This work was funded by the Natural Sciences and Engineering Research Council of Canada and the Canada Research Chair Program. NB acknowledges support from the CQIQC Undergraduate Summer Research Studentships.

[1] U. Weiss, *Quantum Dissipative Systems* (World Scientific, Singapore, 1999).
[2] A. Nitzan, *Chemical Dynamics in Condensed Phases: Relaxation, Transfer, and Reactions in Condensed Molecular Systems* (Oxford, 2006).
[3] A. J. Leggett, S. Chakravarty, A. T. Dorsey, M. P. A. Fisher, A. Garg, and W. Zwerger, Rev. Mod. Phys. **59**, 1 (1987).
[4] K. Le Hur, "Understanding Quantum Phase Transitions," ed. L. D. Carr (Taylor and Francis, Boca Raton, 2010).
[5] A. Dhar, Adv. Phys. **57**, 457 (2008).
[6] J.-S. Wang, J. Wang, and J. T. Lu, Eur. Phys. J. B **62**, 381 (2008).
[7] N. Li, J. Ren, L. Wang, G. Zhang, P. Hänggi, and B. Li, Rev. Mod. Phys. **84** , 1045 (2012).
[8] D. Segal and A. Nitzan, Phys. Rev. Lett. **94**, 034301 (2005); J. Chem. Phys. **122**, 194704 (2005).
[9] H. Wang, M. Thoss, and W. H. Miller, J. Chem. Phys. **115**, 2979 (2001), M. Thoss, H. Wang, and W. H. Miller, J. Chem. Phys. **115**, 2991 (2001).
[10] F. K. Wilhelm, S. Kleff, J. von Delft, Chem. Phys. **296**, 345 (2004), and other papers from Chemical Physics Special Issue on the Spin-Boson Problem, ed. H. Grabert and A. Nitzan, Chem. Phys., **296**, 101-368 (2004).
[11] F. Nesi, E. Paladino, M. Thorwart, and M. Grifoni, Europhys. Lett. **80**, 40005 (2007); Phys. Rev. B **76**, 155323 (2007).
[12] T. C. Berkelbach, D. R. Reichman, and T. E. Markland, J. Chem. Phys. **136**, 034113 (2012).
[13] D. Segal, Phys. Rev. B **73**, 205415 (2006).
[14] L.-A. Wu, C. X. Yu, and D. Segal, Phys. Rev. E **80**, 041103 (2009).
[15] T. Ruokola and T. Ojanen, Phys. Rev. B **83**, 045417 (2011).
[16] J. Thingna, J. L. Garcia-Palacios, and J.-S. Wang, Phys. Rev. B **85**, 195452 (2012).
[17] J. Thingna, J.-S. Wang, and P. Hänggi, Phys. Rev. E **88**, 052127 (2013).
[18] K. A. Velizhanin, M. Thoss, and H. Wang, J. Chem. Phys. **133**, 084503 (2010).
[19] J.-S. Wang, B. K. Agarwalla, H. Li, and J. Thingna, Front. Phys. (2013). DOI 10.1007/s11467-013-0340-x
[20] Y. Vinkler-Aviv, A. Schiller, and N. Andrei, Phys. Rev. B **89**, 024307 (2014).
[21] Y. Yang and C.-Q. Wu, Europhys. Lett. **107**, 30003 (2014).
[22] L. Nicolin and D. Segal, J. Chem. Phys. **135**, 164106 (2011).
[23] D. Segal, Phys. Rev. E **90**, 012148 (2014).
[24] K. A. Velizhanin, H. Wang, and M. Thoss, Chem. Phys. Lett. **460**, 325 (2008).
[25] D. Segal, Phys. Rev. B **87**, 195436 (2013).
[26] K. Saito and T. Kato, Phys. Rev. Lett. **111**, 214301 (2013).
[27] Z. Wang, J. A. Carter, A. Lagutchev, Y. K. Koh, N.-H. Seong, D. G. Cahill, and D. D. Dlott, Science **317**, 787 (2007).
[28] Z. Wang, D. G. Cahill, J. A. Carter, Y. K. Koh, A. Lagutchev, N.-H. Seong, and D. D. Dlott, Chem. Phys. **350**, 31 (2008).
[29] D. Schwarzer. P. Kutne, C. Schroder, and J. Troe, J. Chem. Phys. **121**, 1754 (2004); D. Schwarzer, C. Hanisch, P. Kutne, and J. Troe, J. Phys. Chem. A **106**, 8019 (2002).
[30] V. Botan, E. H. G. Backus, R. Pfister, A. Moretto, M. Crisma, C. Toniolo, P. H. Nguyen, G. Stock, and P. Hamm, Proc. Natl. Acad. Sci. U.S.A. **104**, 12749 (2007).
[31] V. M. Kasyanenko, S. L. Tesar, G. I. Rubtsov, A. L. Burin, and I. V. Rubtsov, J. Phys. Chem. B **115**, 11063 (2011).
[32] B. C. Pein, Y. Sun, and D. D. Dlott, J. Phys. Chem. A **117**, 6066 (2013).
[33] B. C. Pein, Y. Sun, and D. D. Dlott, J. Phys. Chem. B **117**, 10898 (2013).
[34] B. C. Pein and D. D. Dlott, J. Phys. Chem. A **118**, 965 (2014).
[35] G. J. Snyder and E. S. Toberer, Nat. Materials **7**, 105 (2008).
[36] D. M. Leitner, J. Phys. Chem. B **117**, 12820 (2013).
[37] Y. Xu and D. M. Leitner, J. Phys. Chem. B **118**, 7817 (2014).
[38] J. Thingna, J. L. Garcia-Palacios, and J.-S. Wang, Phys. Rev. B **85**, 195452 (2012).
[39] L. G. C. Rego and G. Kirczenow, Phys. Rev. Lett. **81**, 232 (1998).
[40] Y. Meir and N. S. Wingreen, Phys. Rev. Lett. **68**, 2512 (1992).
[41] A. Redfield, Adv. Magn. Reson., 1 (1965).
[42] R. Wertheimer and R. Silbey, Chern. Phys. Lett. **75**, 243 (1980).
[43] C. Aslangul, N. Pottier, and D. Saint-James, J. Physique **47**, 1657 (1986).
[44] M. Zarea, M. A. Ratner, and M. R. Wasielewski, J. Chem. Phys. **140**, 024110 (2014).

[45] H. Dekker, Phys. Rev. A **35**, 1436 (1987).
[46] J. T. Day, The Computer Journal **9**, 394 (1967).
[47] N. Makri and D. E. Makarov, J. Chem. Phys. **102**, 4600 (1995); J. Chem. Phys. **102**, 4611 (1995); N. Makri, J. Math. Phys. **36**, 2430 (1995).
[48] C. Mujica-Martinez, P. Nalbach, and M. Thorwart, Phys. Rev. E **88**, 062719 (2013).
[49] R. P. Feynman and A. R. Hibbs, Quantum Mechanics and Path Integrals (McGraw-Hill, New-York 1965).
[50] N. Makri, J. Chem. Phys. **111**, 6164 (1999)
[51] D. Segal and A. J. Millis and D. R. Reichman, Phys. Rev. B **82**, 205323 (2010); Phys. Chem. Chem. Phys. **13**, 14378 (2011).
[52] L. Simine and D. Segal, J. Chem. Phys. **138**, 214111 (2013).
[53] M. Kulkarni, K. L. Tiwari, and D. Segal, Phys. Rev. B **86**, 155424 (2012), New J. Phys. **15**, 013014 (2013).
[54] A. Mitra and A. J. Millis, Phys. Rev. B **72**, 121102(R) (2005).
[55] S. Weiss, J. Eckel, M. Thorwart, and R. Egger, Phys. Rev. B **77**, 195316 (2008); J. Eckel, F. Heidrich-Meisner, S. G. Jakobs, M. Thorwart, M. Pletyukhov, and R. Egger, New J. Phys. **12**, 043042 (2010).
[56] D. Segal, D. R. Reichman, and A. J. Millis, Phys. Rev. B **76**, 195316 (2007).
[57] N. Makri, J. Phys. Chem. B **103**, 2823 (1999).
[58] The heat current through a single mode (frequency Δ) harmonic junction is given by $j_q = \frac{2}{\pi}\int_0^\infty \hbar\omega\mathcal{T}(\omega)[n_L(\omega)-n_R(\omega)]d\omega$ with $\mathcal{T}(\omega) = \frac{\omega^2\Gamma_L(\omega)\Gamma_R(\omega)}{(\omega^2-\Delta^2)^2+[\Gamma_R(\omega)+\Gamma_L(\omega)]\omega^2}$ [59].
[59] D. Segal, A. Nitzan, and P. Hänggi, J. Chem. Phys. **119**, 6840 (2003).
[60] BR results of Fig. 8 were calculated in the fermionic picture, by following Ref. [25] with the Golden-Rule transition rates evaluated by an explicit integration, to allow the band-edge effects to be properly accounted for. Cutoff effects become more pornounced at high temperaures and large tunneling frequencies, $k_BT/\hbar\omega_c > 0.2$, $\Delta/\omega_c > 0.1$.
[61] J.-S. Wang, Phys. Rev. Lett. **99**, 160601 (2007).
[62] M. Grifoni, M. Winterstetter, and U. Weiss, Phys. Rev. E **56**, 334 (1997).
[63] J. Ren, P. Hänggi, and B. Li, Phys. Rev. Lett. **104**, 170601 (2010).
[64] T. Chen, X. B. Wang, J. Ren, Phys. Rev. B **87** 144303 (2013).
[65] C. Uchiyama, Phys. Rev. E **89**, 052108 (2014).